© Universiti Tun Hussein Onn Malaysia Publisher's Office

IJIE

http://penerbit.uthm.edu.my/ojs/index.php/ijie
ISSN : 2229-838X e-ISSN : 2600-7916

The International Journal of Integrated Engineering

Numerical Study of Ducted Turbines in Shallow Water Environment

Azzim Rosli[1], Anas Abdul Rahman[1,2*], Ayu Abdul-Rahman[3], Najwa Syafiqa Marzuki[1], Wan Muhammad Fadhli[1], Syafiq Misran[1], Ramadhan Ahmed Ramadhan Basiddiq[1]

[1]Mechanical Engineering Program, Faculty of Mechanical Engineering Technology,
Universiti Malaysia Perlis, Pauh Putra Main Campus, 02600 Perlis, MALAYSIA

[2]Institute for Energy Systems, School of Engineering,
University of Edinburgh, Faraday Building, King's Buildings, Colin Maclaurin Road, Edinburgh, EH9 3DW

[3]Department of Mathematics and Statistics, School of Quantitative Sciences,
Universiti Utara Malaysia, 06010 UUM, Sintok, Kedah, MALAYSIA

DOI: https://doi.org/10.30880/ijie.2023.15.07.006
Received 21 September 2022; Accepted 3 October 2023; Available online 5 December 2023

Abstract: The development of tidal turbines, particularly for shallow water applications, is still in its early stages. Vertical axis tidal turbines (VATT) are often preferred for shallow water due to the bidirectional nature of tidal currents. Implementing a channelling system around a tidal turbine can significantly stabilise the flow field, increase the current velocity, and enhance the energy efficiency of the turbine. However, there has been limited exploration of using channelling techniques to improve the performance of VATTs in turbid areas. This study employs a numerical analysis using computational fluid dynamics (CFD) to investigate VATTs. The VATT model is represented by a cylindrical object with a diameter and height of 5 meters. The simulation focuses on the wake characteristics and the design of turbine arrays. The Reynolds-Averaged Navier-Stokes (RANS) equations are utilised as flow viscous solvers in ANSYS Fluent, and the effectiveness of the ducts in energy conversion is calculated using the realizable two-layer k-ε turbulence model. The primary objective of this study is to examine the impact of converging devices on tidal turbine performance and propose an optimal design for shallow water applications. The proposed ducted design shows an increase in current speed passing through the device by 11.1%. Although the wake generated by the multi-row staggered array layout disperses the flow to the side of the domain, the model demonstrates a 0.9% improvement in velocity magnitude. Conversely, the results for the single-row inline layout indicate the most favorable arrangement for shallow water applications, with a 19.4% increase in velocity magnitude and a shorter wake generation.

Keywords: Tidal energy, vertical axis tidal turbine, grid sensitivity analysis, array layout

1. Introduction

Malaysia is a country that largely uses fossil fuels to produce energy. Because of the population and economic growths, industry development, technological advancements, and rising living standards, the country's energy sector is growing year after year. Due to this reason, the Malaysian government has started shifting their focus to renewable energy

*Corresponding author: anasrahman@unimap.edu.my

sources in order to reduce the dependency on hydrocarbons [1]. Despite the challenges faced by the coronavirus outbreak, Malaysia's utilization of the renewable energy industry is expected to grow in the coming decades. Numerous factors are needed to stimulate interest and development in renewable energy sectors, though none is more important than the policies and initiatives by the government [2]. Malaysia is united with all other global leaders in endorsing the programme in 2030 for Sustainable Development, which is a worldwide pledge to be even more responsible, robust, and rapidly improving, with 17 Sustainable Development Goals (SDGs) and 169 ambitions outlined [3].

In the field of renewable energy, tidal is considered a relatively new resource. Notably, the main way to turn tidal energy into power is through tidal turbines. Similar to wind turbines, tidal turbines may be classified into two types, namely vertical axis tidal turbines (VATT) and horizontal axis tidal turbines (HATT). Since the kinetic energy of the flow stream is proportional to the cube of the current flow velocity, the flow velocity is the most important factor in producing power from tidal currents [4]. Tidal turbines come in a wide variety of designs, but several things need to be considered when selecting the best one to produce energy effectively. Current speed, top and bottom clearance, and deployment depth are among the elements that need to be taken into account. Even though not often employed in commercial sites, ducted systems have lately undergone some major advances. For instance, unidirectional and bidirectional ducts are types of converging devices utilised around a turbine rotor and have been outfitted on various prototypes.

Due to the generated physical phenomena, both methods have been taken into consideration to improve a turbine's performance beyond flow velocity together with the structure [5]. This article aims to investigate the influence of converging devices on the wake generation, and also to propose an optimal converging device design for shallow water applications. A study by Hua-Ming et al. [6] highlighted the importance of the duct's interior wall design in improving its efficiency for energy conversion. Significantly, results from this study also demonstrate that the interior wall is a variable that can significantly affect the efficiency of tidal turbines, which agrees with a study conducted by Jo et al. [7]. For the current work, a turbine model with a diameter of 5.0 meters was constructed and tested with two duct designs to improve the wake turbulence downstream of the devices.

2. Simulation

2.1 Boundary Condition

Based on previous studies conducted by Rahman et al. [8] and Suhri et al. [9], the simulation method employed the following boundary conditions: initial velocity (U_o) set at 1 m/s [10]-[13], density (ρ) at 1023 kg/m^3, and dynamic viscosity (μ) at 0.00092 Ns/m^2. The ducted device was positioned 12.5D meters away from the domain's inlet, as depicted in Fig. 1. In this work, D represents the turbine diameter. Fig. 1(b) illustrates that the depth of the domain was 6D (i.e., 6 x 5 meters = 30 meters), which adequately represents the shallow water conditions in the vicinity of Malaysia [14].

The ducted device was designed using SOLIDWORKS, while the domain was created using ANSYS Design Modeller. Subsequently, grid sensitivity analysis was performed after defining the Inlet, Outlet, and Top walls. The simulation utilised a realizable two-layer k-ε turbulence model based on Reynolds-Averaged Navier-Stokes (RANS) equations. The turbulence intensity of 5% was set for both the inlet and outlet boundaries. The top wall boundary condition was specified as shear. To ensure accurate convergence, a second-order upwind scheme was employed for momentum, turbulent kinetic energy, and turbulent dissipation energy at the boundary cells, as it provides more precise results compared to the first-order scheme. The residual absolute criterion value was set to 1e-06, and a standard initialisation was computed. The simulation ran for 500 iterations, with convergence achieved after 300 iterations.

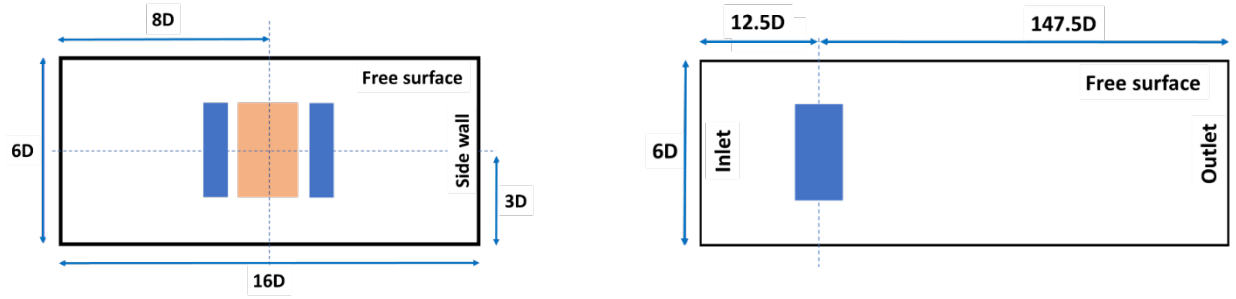

(a) Front view (b) Side view

Fig. 1 - Device placement inside the domain

2.2 Modelling

The duct's cross-sectional area decreases gradually from the entrance to the front of the turbine, while it increases progressively from the rear end of the turbine to the outlet. This configuration allows for the calculation of tidal current energy, as the flow velocity increases steadily when the cross-sectional area of the ducts fore body decreases. Furthermore, as the cross-sectional area of the duct's body progressively increases, the flow velocity in the wake can be

reduced, leading to a more stable wake flow field and preventing boundary layer separation. The design of the two ducting configurations in

Fig. **2** incorporates parameters obtained from earlier research conducted by Huang Ming et al. [6],[8]. This study aimed to conduct a numerical simulation to analyse the 3D viscous flow environment around the duct of a vertical axis current turbine. Specifically, the focus was on observing the flow velocity within the duct and considering velocity fluctuations. The placement of the ducted tidal turbine within the domain is illustrated in **Error! Reference source not found.**, and the dimensions of the domain can be found in **Error! Reference source not found.**. While previous studies by Borg et al. [5], [9] have explored the effectiveness of the ducted tidal current turbine, they did not specifically analyse the function of the duct. In this study, the viscous flow field surrounding the duct was modelled using the Reynolds-Averaged Navier-Stokes (RANS) equations and continuity equations, implemented through ANSYS Fluent. Notably, grid sensitivity analysis was performed to determine an appropriate mesh element size for the simulation.

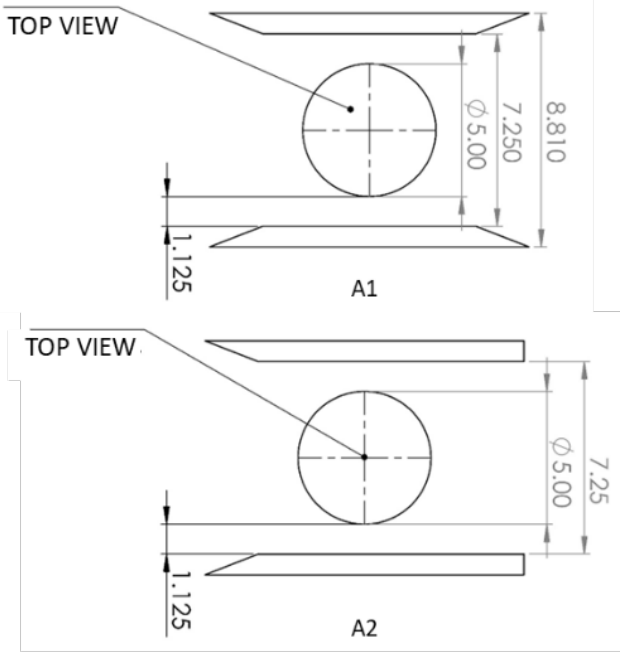

Fig. 2 - Cross section of the ducting designs employed in the current work

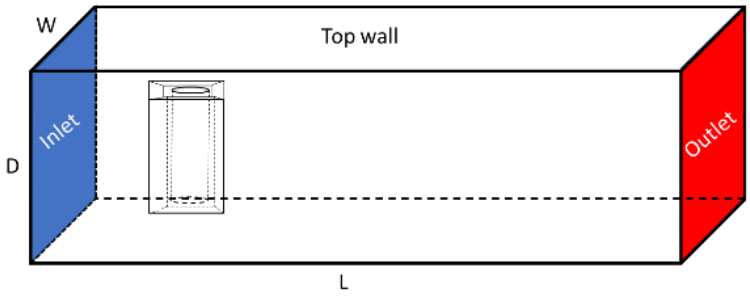

Fig. 3 - Computational domain

Table 1 - Domain parameters

Parameters	Value
Length of the domain, L	800 m
Width of the domain, W	80 m
Depth of domain, D	30 m

In order to capture flow fluctuations accurately, a denser mesh is preferred and considered more desirable. However, it's important to note that using a very small element size or a dense mesh requires higher computational resources, resulting in longer calculation times. As the level of mesh refinement increases, the impact of further refinement on numerical results diminishes. To enhance the quality of the mesh elements, the inflation refinement method was employed in this study. The transition ratio was set at 0.3 m, similar to face sizing, with a maximum growth of five layers.

Furthermore, an inflation option with a growth rate of 1.2 was selected. Five different refinement values were evaluated, as summarised in Table 2, with the very fine and very coarse settings yielding approximately 5,367,000 and 771,000 elements, respectively.

Furthermore, the results of the sensitivity analysis are depicted in Fig. 4, where the velocity values were extracted from the centre of the object at a distance of 12D downstream. It can be observed that the 'Fine' mesh configuration yielded the highest maximum velocity (0.882038 m/s) at a reasonable computational cost. Therefore, this mesh setup was selected for subsequent simulations.

Fig. **5** illustrates the element size in the domain, which was set to 2.0 meters, while the faces and edges were set at 0.3 meters and 0.25 meters, respectively. The fine mesh refinement with inflation exhibited a positive skewness distribution, with a mean skewness value of 0.38, which is considered highly acceptable.

Table 2 - Grid sensitivity analysis of ducted VATT

Type	Element number
Very Fine	5.367 x 10^6
Fine	2.474 x 10^6
Medium	1.452 x 10^6
Coarse	1.000 x 10^6
Very Coarse	0.771 x 10^6

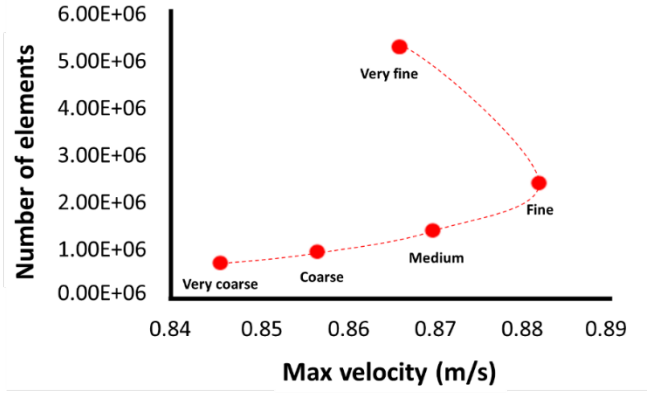

Fig. 4 - Maximum velocity plotting with number of elements

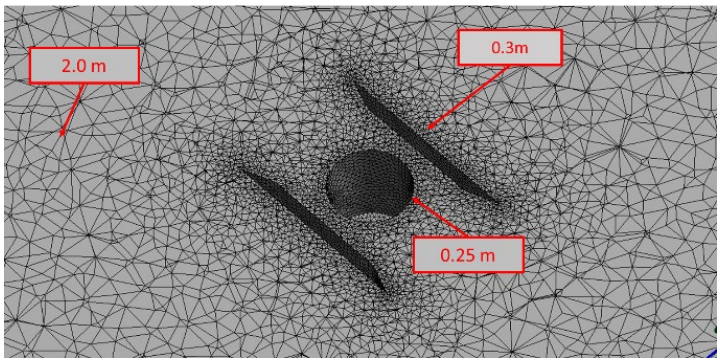

Fig. 5 - Fine mesh with inflation refinement

2.3 Analysis

2.3.1 Tidal Stream Energy Conversion Theory

The power generated by a tidal current turbine can be determined using various formulas available for wind energy calculations. The only difference in these formulas lies in the density values used for tidal and wind sources. Therefore, the expression for the power generated by the tidal stream current can be given as follows [15]:

$$P = \frac{1}{2}\rho A v^3 \tag{1.1}$$

where ρ is the density of the fluid, A is the area of the turbine rotor and v is the velocity of the fluid. The HATT and the VATT have different cross-sectional areas, A. In the case of the VATT, the cross-sectional area is:

$$A = H \times \mathrm{D} \tag{1.2}$$

The VATT is equal to the height (H) multiplied by the diameter (D) of the rotor. Because of some losses, the tidal current can harvest a part of this power, and the formula can be modified as follows [16]:

$$P = \frac{1}{2} C_p \rho A v^3 \tag{1.3}$$

where C_p is the power coefficient. Tidal turbine efficiency, η, can then be calculated using the following expression:

$$\eta = C_p \times 100\% \tag{1.4}$$

2.3.2 Governing Equation of Incompressible Viscous Flow

It is possible to formulate the incompressible fluid continuity equation as follows:

$$\frac{\partial u}{\partial x} + \frac{\partial v}{\partial y} + \frac{\partial w}{\partial z} = 0 \tag{1.5}$$

where the velocity components in the X, Y, and Z directions are denoted by $u, v,$ and w, respectively. For the transfer of momentum, Reynolds-Averaged Navier-Stokes (RANS) equations are as follows:

$$\rho \frac{\partial \overline{u_i}}{\partial t} + \rho \overline{u_j} \frac{\partial \overline{u_i}}{\partial x_j} = -\frac{\partial \bar{p}}{\partial x_i} + \frac{\partial}{\partial x_j} (\mu \frac{\overline{u_i}}{\partial x_j} - \rho \overline{u_i' u_j'}) \tag{1.6}$$

where p is time-averaged relative pressure, $-\rho \overline{u_i' u_j'}$ is the Reynolds stress tensor, ρ is the liquid density, and μ is the liquid's dynamic viscosity.

2.3.3 Turbulence Intensity

The intensity of turbulent (TI_x) flow is defined as relative to the mean incidence velocity U_o as [17]:

$$TI_x = \frac{\sqrt{(u_x - U_x)}}{U_o} \tag{1.7}$$

where $u_x$is the value of velocity on the x-axis plane, U_x is the velocity magnitude and U_o is the initial velocity.

3. Result and Discussion

Data validation is a crucial step in ensuring the reliability and accuracy of generated data. It involves assessing the quality and reliability of a data source before utilizing, importing, and processing the data. In the context of this research, Table 3 presents the published data that was used for validating and verifying the simulated results. It is important to note that while Stallard et al. [17] used a transient approach in their work, this study employed a steady flow method due to computational constraints.

Table 3 - Details on the validation data used in this study

Experimental Data*	Comparison of single devices with research findings from Clary *et al.* [18]
Experimental Data**	Comparison of multi-row staggered array devices with research findings from Stallard *et al.* [17]
Experimental Data***	Comparison of single-row inline devices with research findings from Olczak *et al.* [19]

3.1 Comparison Between Ducted and Non-Ducted VATT

This study focuses on examining the progression of wake turbulence throughout the domain. By analysing the velocity contour, it is possible to identify the wake characteristics at different locations, both near and far from the turbine. Fig. 6 illustrates that the side of the cylinder experiences the highest velocity. As the flow passes through a non-ducted turbine, the velocity decreases initially and then rapidly increase again. The merging of the wake occurs at a shorter distance. There is a noticeable decrease in velocity from 1 m/s to 0.98 m/s after a certain distance, which is caused by an accumulation of wakes resulting in a stagnant area, as shown in Fig. 6(b). The velocity recovery for the non-ducted turbine ranges from 0.8 m/s to 0.98 m/s before returning to the original velocity. In Fig. 7, the separated wake generated by the ducted turbine (A1) and the point of merging can be observed. This phenomenon can be attributed to the section of the duct wall responsible for guiding the water flow. The transition from varied velocities to a uniform flow velocity takes a significant amount of time. The velocity recovery range for ducted design A1 is 0.8 to 1 m/s, while the region between the duct wall and the turbine exhibits the highest velocity.

After passing through the ducted turbine, the water's velocity decreases to 0 m/s and then gradually increases back to its initial velocity. Ducted turbines exhibit a maximum velocity of 1.8 m/s, distinguishing them from non-ducted turbines. Fig. 7 and Fig. 8 reveal that both converging devices have similar interior designs for the inlet, aimed at capturing more tidal current and directing it towards the device. Minor modifications were made to improve the generated wake, including slight changes at the end of the interior wall for both designs. However, design A2 features a straight panel instead of a diffuser design like A1, specifically at the rear interior duct. The maximum velocity for ducted design A2 is 2 m/s, while the minimum velocity is 0 m/s. The area between the wall duct and the turbine exhibits the highest velocity, as depicted in Fig. 8. Similar to ducted design A1, the velocity decreases to 0 m/s and eventually returns to its original value. The merging of the wake takes less time compared to ducted design A1, but more time compared to the non-ducted turbine. In terms of velocity, non-ducted turbines have higher values compared to ducted design A2, where the maximum velocities observed are 2.2 m/s, 2 m/s, and 1.8 m/s. Various wake characteristics were observed between the two designs.

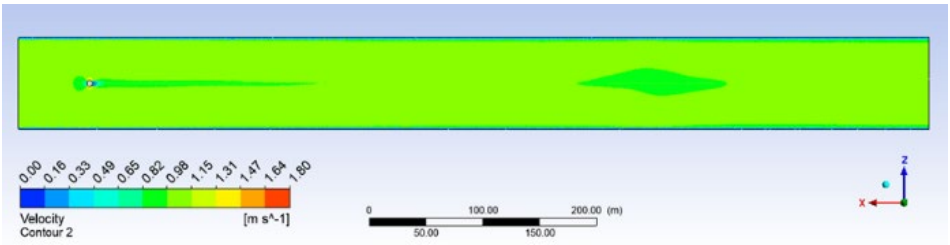

(a) Velocity contour of the full domain for non-ducted model (cylindrical object)

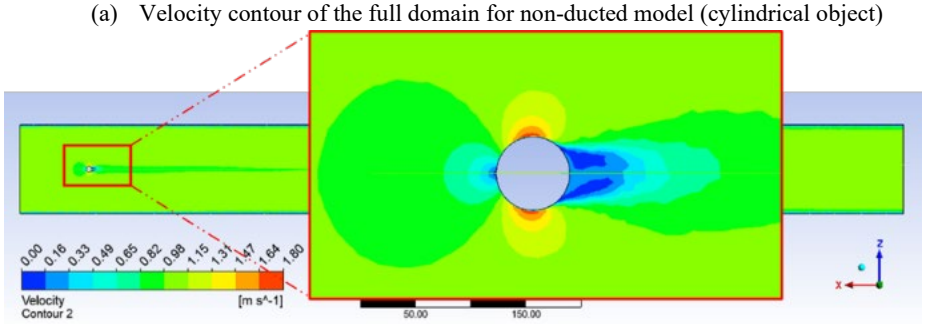

(b) Close up view of the velocity contour for non-ducted (cylindrical object)

Fig. 6 - Velocity contour of non-ducted model (cylindrical object)

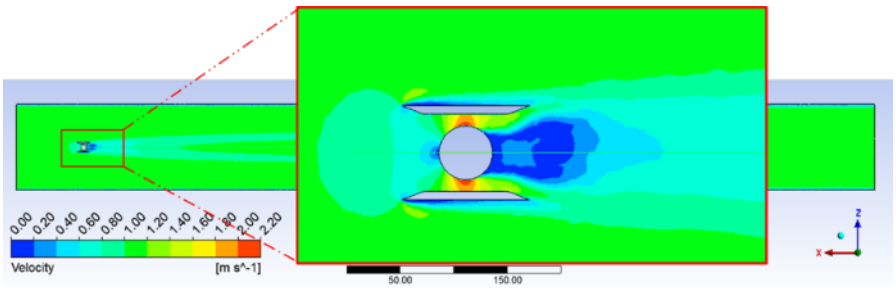

Fig. 7 - Velocity contour of ducted A1

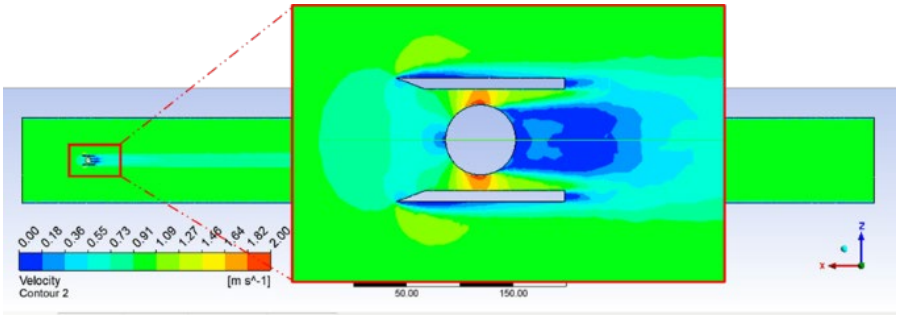

Fig. 8 - Velocity contour of ducted A2

According to a previous study conducted by Clary et al. [18], it was observed that as the distance increased, the velocity gradually returned to its initial value. In the case of the non-ducted design, the velocity magnitude plot displayed a bimodal distribution. This phenomenon is a result of the height input in the CAD model, leading to varying velocity magnitudes at the top and bottom of the cylinder. Based on Fig. 9(a), the peak velocity magnitudes are 0.65 m/s for ducted design A1, 0.69 m/s for ducted design A2, and 0.85 m/s for the cylinder. The percentage deviation, as shown in **Error! Reference source not found.**, is negative, indicating that the simulation data exceeds the experimental data due to differences in domain and device characteristics. At a distance of 8D downstream, the maximum velocities observed are 0.73 m/s for ducted design A1, 0.7 m/s for ducted design A2, and 0.87 m/s for the non-ducted turbine, as depicted in Fig. 9(b). It is apparent that there is a slight increase in velocity from 6D to 8D.

Furthermore, it can also be seen that the percentage deviation decreases, indicating that the flow velocity is approaching the freestream velocity, as shown in **Error! Reference source not found.**. At 12D downstream, the highest velocities are 0.88 m/s for ducted design A1, 0.72 m/s for ducted design A2, and 0.96 m/s for the non-ducted turbine. All devices exhibit a significant increase in velocity from 6D to 12D. The wake of the non-ducted turbine begins to recover at 12D, while ducted design A1 shows a gradual recovery, and ducted design A2 requires a greater distance for recovery. Similar to the observations at 8D, the percentage deviation at 12D, shown in **Error! Reference source not found.**, decreases, indicating a closer alignment of the flow velocity with the freestream velocity. Considering these results, it can be inferred that using individual ducted turbines with the A2 design may not be suitable for implementation in an array for shallow water applications, as subsequent devices downstream of the array could be significantly affected by the slow-moving current.

Table 4 - Percentage deviation at 6D

	Simulation	Experiment*	Percentage Deviation (%)
A1	0.66		-34.36
A2	0.69	0.9	-31.12
Cylinder	0.85		-14.77

Table 5 - Percentage deviation at 8D

	Simulation	Experiment*	Percentage Deviation (%)
A1	0.73		-27.10
A2	0.70	0.92	-30.01
Cylinder	0.87		-12.93

Table 6 - Percentage deviation at 12D

	Simulation	Experiment*	Percentage Deviation (%)
A1	0.88		-11.7962
A2	0.72	0.98	-28.3222
Cylinder	0.97		-3.1332

3.2 Multi-Row Staggered Array Configuration

To examine the interaction between multiple ducted turbines, a simulation was conducted using a setup similar to the one described in Olczak et al.'s study [19]. The study in [19] observed a 20% increase in individual rotor thrust, prompting the investigation of a seven-turbine array. The turbines were arranged in a staggered pattern with a lateral

spacing of 1.5 times the rotor diameter (D) and a longitudinal spacing of 8 times D, as shown in Fig. 10. This configuration allowed for a comparison between the multi-row boundary condition and the design of a single ducted turbine.

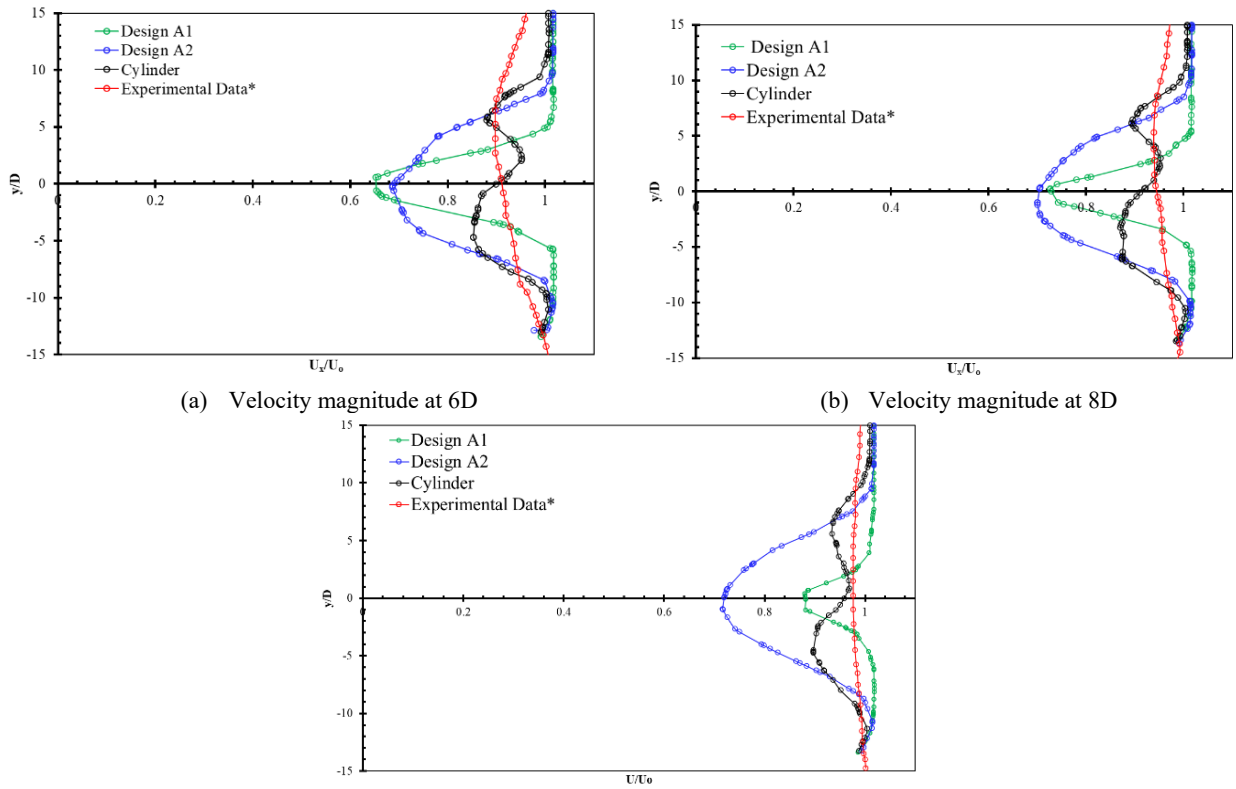

(a) Velocity magnitude at 6D

(b) Velocity magnitude at 8D

(c) Velocity magnitude at 12D

Fig. 9 - Comparison of maximum velocity magnitude between the proposed design and published data

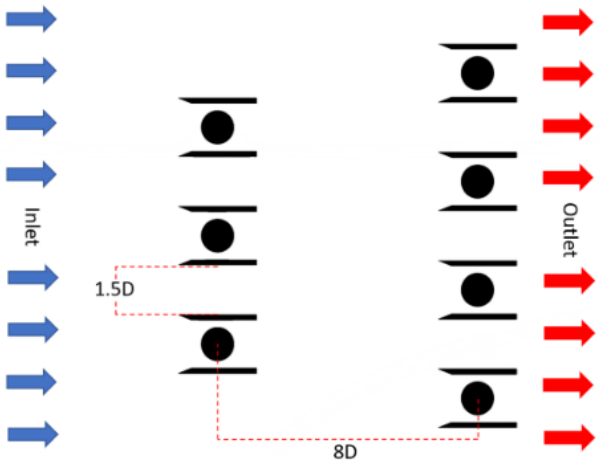

Fig. 10 - Staggered array setup

The second row of turbines, consisting of four ducted devices, initially has a flow velocity of 0.61 m/s. As it moves a few meters, the velocity increases to 0.81 m/s. However, instead of merging, the wake scatters to the side wall of the domain, as shown in Fig. 11(a). This may be due to the insufficient width of the domain to display the combined wake. Interestingly, the velocity contour profile in Fig. 11(b) demonstrates that the staggered array conforms to the expected velocity profile. The deep blue and light blue areas indicate higher velocity when the flow encounters the turbine surface, followed by a decrease in velocity after passing through the turbine. The collision of high-velocity flow with the turbine surface results in energy loss, creating a low-velocity region behind the turbine. Based on Fig. 11(b), it can be inferred that the velocity outside the wake in a closed channel must be much higher than the free stream to maintain volume flow

rate continuity, since the average wake velocity is lower than the free-stream velocity. This effect causes the flow to rise around the tidal current turbine [20].

According to Fig. 11(b), the maximum velocity for the first row of turbines is 2.02 m/s, but it should be noted that the maximum speed reaches 2.22 m/s. This increase is visible in the space between the second-row turbine and the wall duct, as the narrow gap enhances velocity. The green region behind the turbine elongates as it traverses the velocity contour of the domain in a staggered pattern. The turbulent mixing leads to slower velocities, which delays the recovery of the downstream wake. Consequently, the limited clearance between the duct wall and turbine hinders the smooth flow of kinetic energy, resulting in excessive energy dissipation at the end of the wall duct, as illustrated in Fig. 12. A small area of red colour, indicating a value of 0.1 m^2/s^2, indicates high kinetic energy for the A2 ducted design. It should be noted that the velocity is 0.1 m/s per second. The high velocity causes the flow from the three cylinders in the first-row turbines to merge in the close wake of the second-row turbine. Even with increased longitudinal spacing between each row, the velocity takes longer to stabilise.

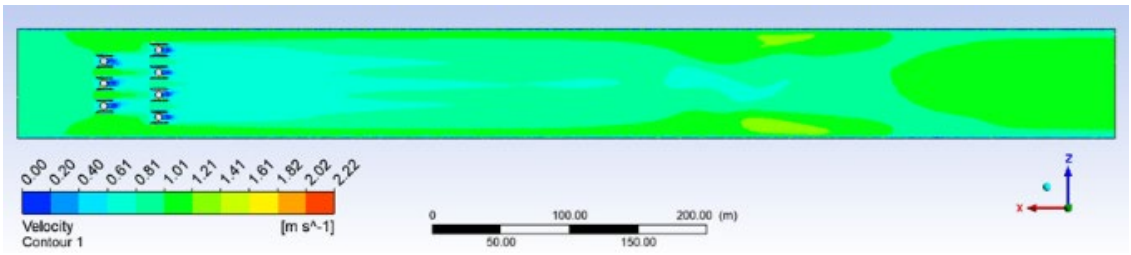

(a) Full domain

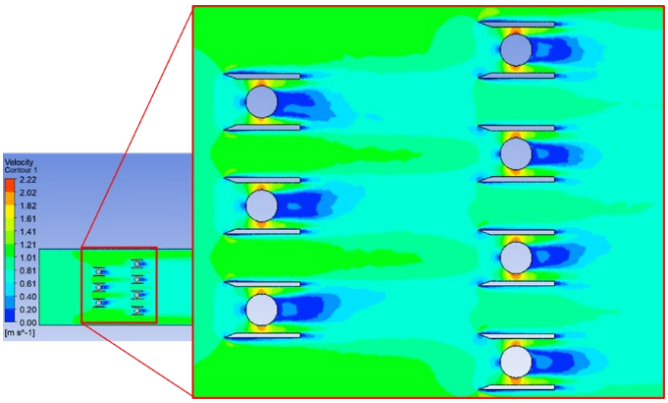

(b) Close up view

Fig. 11 - Velocity contour for the multi-row staggered array

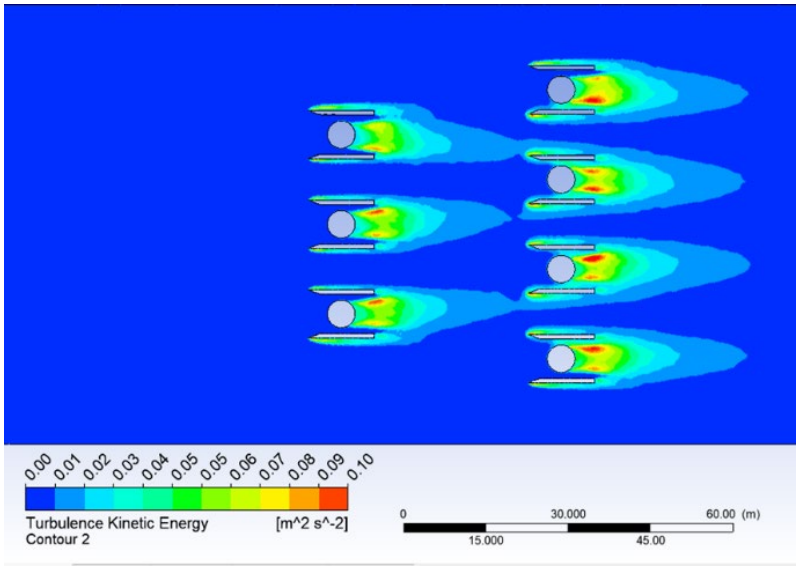

Fig. 12 - Turbulence kinetic energy contour of the multi-row staggered array

Through a comparison between the experimental findings by Olczak et al. [19] at a downstream velocity of 10D and the staggered array depicted in Fig. 13, it is observed that the lowest velocity for ducted design A2 is 0.26 m/s. The experimental results exhibit the highest fluctuations around the right peak. By examining the data, it can be inferred that the velocity of ducted design A2 is lower than the experimental data at the 10D position. The mean absolute error (MAE) at a downstream position of 10D is 0.3, considering the 38 data points shown in Fig. 13. These findings indicate that the velocity with ducted design A2 is relatively low at these downstream locations. Moving to a downstream position of 12D, as depicted in Fig. 14, the velocity begins to increase, with the lowest recorded value being 0.66 m/s. However, the velocity for ducted design A2 at 12D is still lower than the corresponding experimental data, indicating a growing deviation between the two. This suggests that as the downstream distance increases, it takes more time for the fluid flow to stabilise and fully recover from the wake effects. The MAE at 12D downstream is 0.26, which shows a decrease from 10D to 12D, reaching a value of 0.04. This decrease can be attributed to the flow moving further away from the devices and starting to recover.

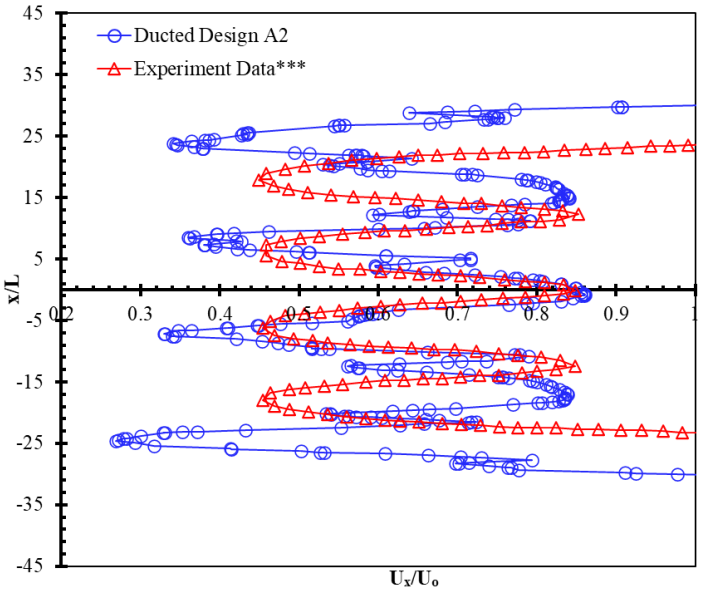

Fig. 13 - Velocity magnitude at 10D of the multi-row staggered array

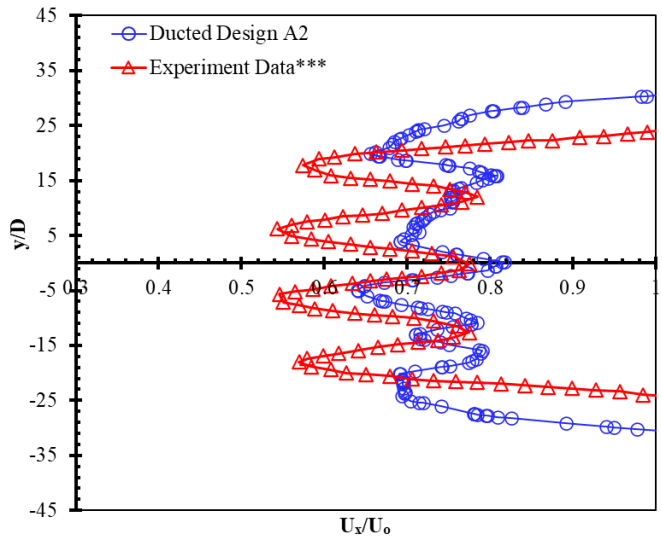

Fig. 14 - Velocity magnitude at 12D of a multi-row staggered array

3.3 Single-Row Inline Configuration

Using the same mesh refinement with inflation and soft behaviour, a model was created consisting of a single row of three turbines, following the arrangement discussed earlier.

Fig. **15** illustrates the configuration of the inline layout, where each ducted turbine is positioned with a lateral spacing of 1.5 times the rotor diameter (1.5D) from the adjacent ducted walls. Fig. 16 reveals that the wake recovery of the top

ducted turbine is the fastest compared to the middle and bottom ducted turbines. This is evident from the shorter length of the light green region, representing a velocity of 0.86 m/s. In contrast, both the middle and bottom ducted turbines exhibit slower velocity recovery, indicated by the longer length of the light green region. The inline layout aligns with the fundamental velocity profile as shown by the velocity contour, similar to the staggered array. Furthermore, Fig. 16 demonstrates higher velocity upon impact with the turbine surface and a lower velocity after passing through the ducted turbine. The maximum velocity achieved in the single-row inline array is 2.15 m/s, which is lower than that of a multi-row array.

Fig. 17 highlights the dissipation of excess energy at the end of the wall duct due to the restricted passage of turbulent kinetic energy between the duct wall and the turbine. For the ducted design A2, a small red region with a value of 0.09 m^2/s^2 indicates high kinetic energy. This value is 0.01 m^2/s^2 lower than that observed in the multi-row staggered layout. The diminished kinetic energy can be attributed to the fact that a significant portion of the flow's energy has already been dispersed throughout the curved structure of the cylinder turbine. In order to assess the viability of the single-row inline layout arrangement, a comparative study was conducted by comparing the numerical data obtained from the modelled simulation with the results of small-scale tests performed by Stallard et al. [17].

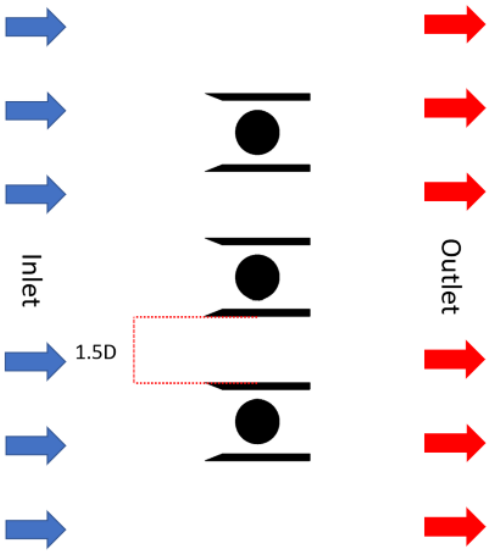

Fig. 15 - Inline setup

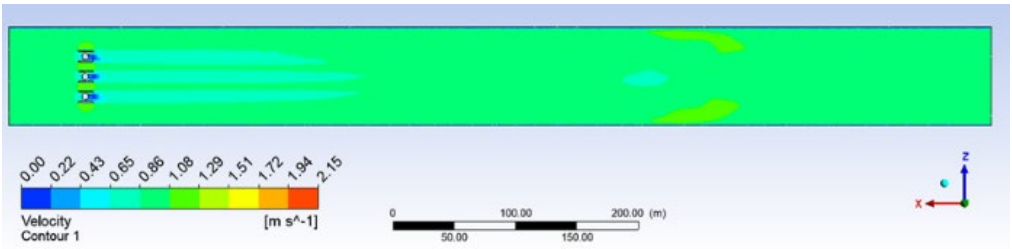

(a) Full domain view

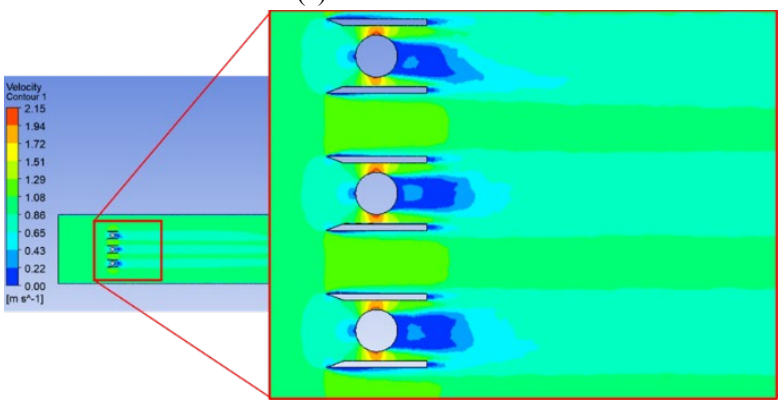

(b) Close up view

Fig. 16 - Velocity contour of inline configuration

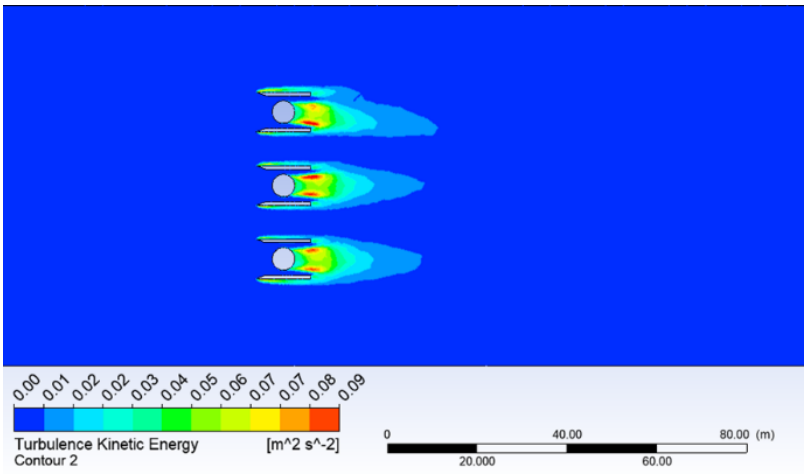

Fig. 17 - Turbulence kinetic energy contour of single row inline configuration

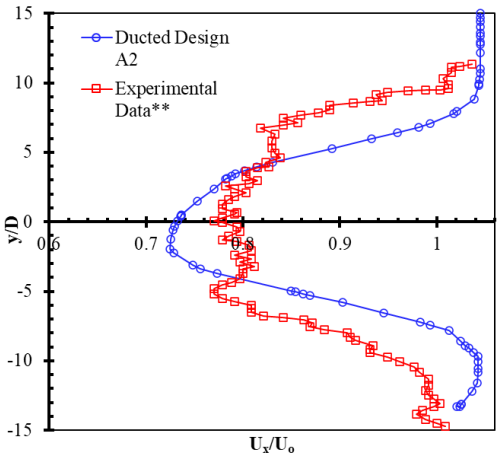

(a) Velocity magnitude at 8D

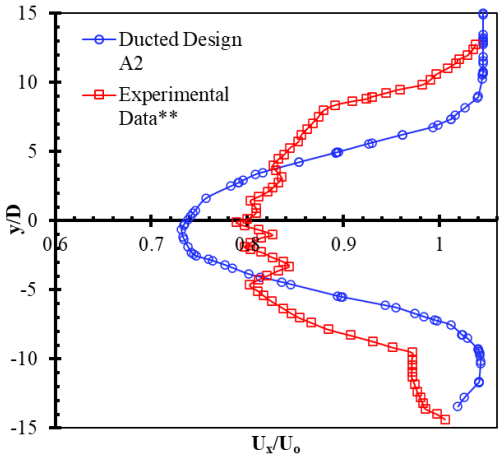

(b) Velocity magnitude at 10D

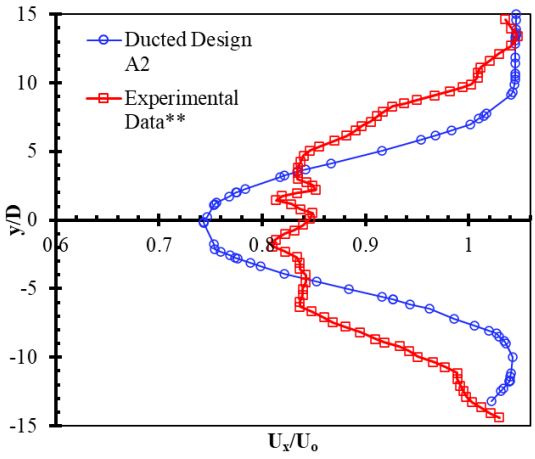

Velocity magnitude at 12D

Fig. 18 - Velocity magnitude at 8D, 10D, and 12D of single row inline configuration

By analysing Fig. 18, which compares experimental data at 8D, 10D, and 12D downstream with the modelling data, it can be observed that the wakes from the single-row inline turbine did not merge to form a single wake further downstream. Individual wakes are still discernible at the 12D position. The maximum simulated velocities at 8D, 10D, and 12D are recorded as 0.72 m/s, 0.73 m/s, and 0.74 m/s, respectively. The presence of the turbine between the ducts creates a local blockage, resulting in a high-velocity bypass flow between them. This can be inferred from the distribution of streamwise velocity after the approach flow encounters the turbines. The mean absolute error (MAE) between the

simulated and experimental values of velocity, as depicted in the velocity chart in Stallard et al. [17], is 0.08 at 8D, which is comparable to the MAE at 10D. At 12D, the MAE drops to 0.07. Across each cross-section, the turbulence remains relatively constant regardless of water depth. Fig. 19 shows that the turbulence intensity (TI_x) measures 1.45 at 8D, 1.46 at 10D, and continues to increase to 1.49 at 12D. This suggests that the rate of momentum recovery slows down as the downstream distance increases. If the turbulence intensity remained constant, the wake zone may not have extended as much. Additionally, the turbulence intensity begins to decrease as velocity increases. Similar to the previous observation, the turbulence intensity value decreases as velocity increases, as velocity and turbulence intensity are inversely related.

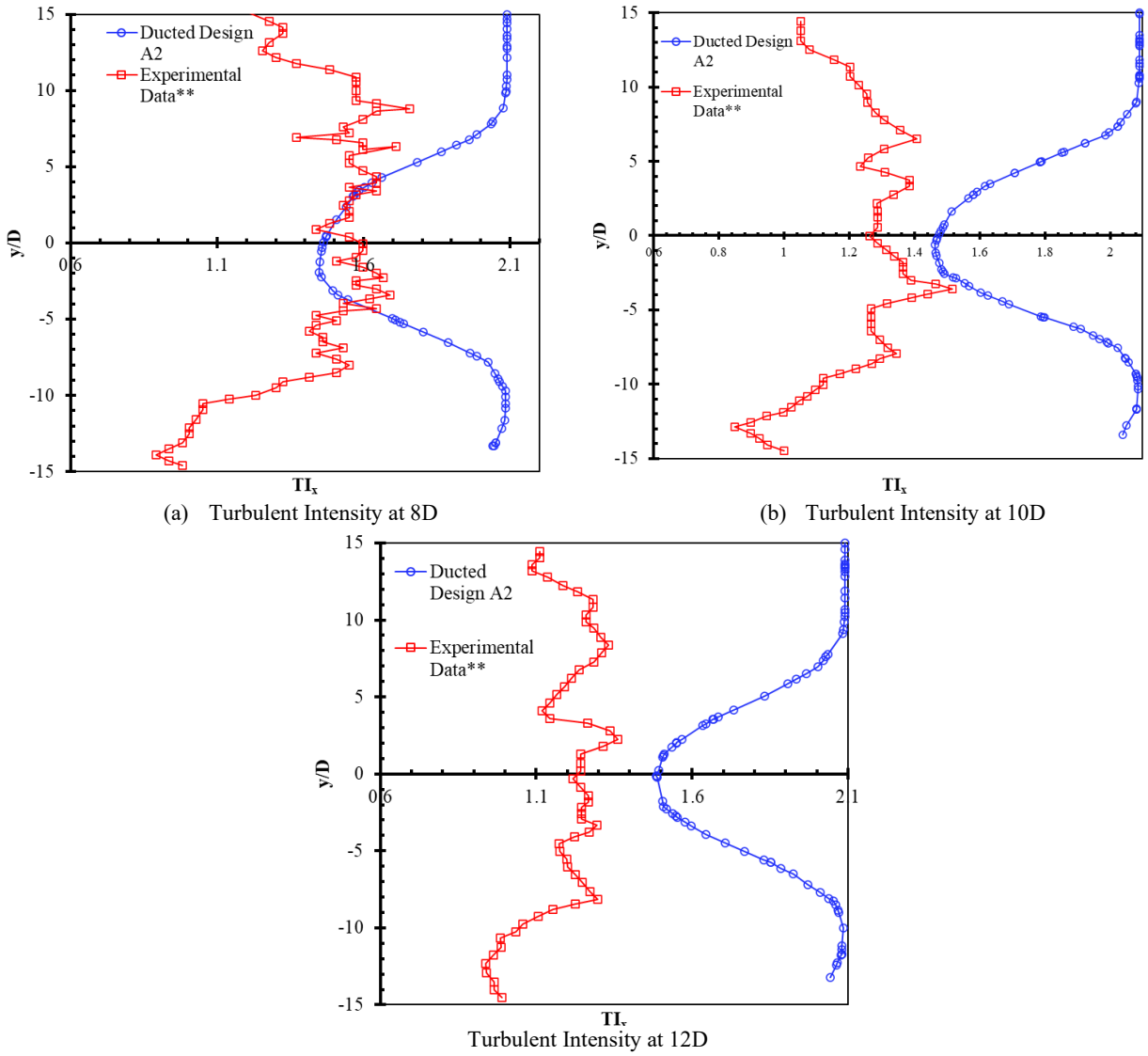

Fig. 19 - Turbulence intensity of single row inline configuration at three downstream distances

At a distance of 8D, both the ducted design A2 and Experimental Data** demonstrate the lowest absolute error, measuring at 2.46%. This can be attributed to the direct relationship between velocity and turbulence intensity observed in both datasets at this specific distance. Therefore, the lower inaccuracy can be explained by this correlation. Fig. 19(a) visually depicts this result, with one marker stacked on top of another. Moving to 10D, Fig. 19(b) indicates the lowest absolute inaccuracy at 8.74%. This suggests that as the flow moves farther away from the tidal devices, both velocity and turbulence intensity gradually decrease. It implies that the turbulence intensity in the Experimental Data** is lower compared to the ducted design A2. As a result, it becomes possible to analyse the discrepancies between the plots of the Experimental Data** and the ducted design.

At a distance of 12D, the minimum absolute inaccuracy is registered at 18.6%. This can be ascribed to the gradual reduction in velocity as the flow moves farther away, leading to a decrease in turbulence intensity. In Fig. 19(c), the gap between the two plots appears wider ($\Delta TI_x \approx 0.3$) compared to the distances of 8D and 10D. This suggests that the turbulence intensity in the Experimental Data** is lower than that in the simulation data. The discrepancy between the experimental and simulation results progressively increases from 0.45 at 8D to 0.57 at 10D, and further to 0.63 at 12D.

This elevated error can be attributed to the utilization of different simulation methods. For instance, this study employed the steady flow approach, while the Experimental Data** was obtained from work employing a transient flow method.

4. Conclusion

The performance of ducted designs A1 and A2 in comparison to a single non-ducted turbine showed significant improvements in term of the incoming velocity experienced by the device. Ducted design A1 achieved a velocity amplification of 22.2% but suffered from a diverging wake pattern. Ducted design A2, on the other hand, demonstrated an 11.1% velocity increase and improved wakes, with similar wake recovery to A1. The proposed convergence device design successfully prevented wake divergence caused by amplified velocity in shallow water applications. Ducted turbines generally outperformed non-ducted turbines, although they had slower wake recovery. The multi-row staggered turbine combined with ducted designs showed superior velocity performance and lower mean absolute error (MAE) values at 10D and 12D compared to the single-row inline turbine. However, the merging of wakes in the multi-row staggered arrangement was unfavourable for shallow water conditions. For shallow water installations, shorter wake generation is preferred to maintain turbine performance. The single-row inline arrangement proved most effective, achieving a 7.5% velocity increase compared to A2, generating shorter wakes, and exhibiting the smallest MAE at 8D, 10D, and 12D. Overall, the straight interior wall duct exhibited superior performance, achieving the goals of investigating convergence devices' impact and proposing the best design for shallow water applications.

Acknowledgement

The authors gratefully acknowledge the support received from the Ministry of Higher Education Malaysia through the Fundamental Research Grant Scheme for Research Acculturation of Early Career Researchers (FRGSRACER) RACER / 1 / 2019 / TK07 / UNIMAP/1. Additionally, the authors are also thankful for the support received from Universiti Malaysia Perlis, specifically from the Research Management Centre (RMC).

References

[1] F. S. Mohd Chachuli, N. Ahmad Ludin, M. A. Md Jedi, and N. H. Hamid, "Transition of renewable energy policies in Malaysia: Benchmarking with data envelopment analysis," *Renewable and Sustainable Energy Reviews*, vol. 150, Oct. 2021, doi: 10.1016/j.rser.2021.111456.

[2] Arnis Abdul Rashid, Edzwan Suwaji, Syeikh Mohd Iqbal Mohd Yusof, and Siti Aisyah Nabilah Suwardi, "Transitioning The Nation Towards Sustainable Energy Malaysia: Working together to achieve sustainability," *Tri-annual Publications*, Kuala Lumpur, p. 12, 2021. Accessed: Jan. 10, 2022. [Online]. Available: http://www.seda.gov.my/wp-content/uploads/2021/07/Vol5_Issue11.pdf

[3] "Sustainable Development Goals," *Economic Planning Unit*, Jul. 12, 2021. Accessed: Jan. 10, 2022. [Online]. Available: https://www.epu.gov.my/en/sustainable-development-goals

[4] S. L. Ward, "8.07 - Tidal Stream Energy," in *Comprehensive Renewable Energy (Second Edition)*, T. M. Letcher, Ed. Oxford: Elsevier, 2022, pp. 104–122. doi: https://doi.org/10.1016/B978-0-12-819727-1.00096-0.

[5] M. G. Borg, Q. Xiao, S. Allsop, A. Incecik, and C. Peyrard, "A numerical performance analysis of a ducted, high-solidity tidal turbine," *Renew Energy*, vol. 159, pp. 663–682, Oct. 2020, doi: 10.1016/j.renene.2020.04.005.

[6] W. Hua-Ming, Q. Xiao-Kun, C. Lin, T. Lu-Qiong, and W. Qiao-Rui, "Numerical study on energy-converging efficiency of the ducts of vertical axis tidal current turbine in restricted water," *Ocean Engineering*, vol. 210, Aug. 2020, doi: 10.1016/j.oceaneng.2020.107320.

[7] C. H. Jo, D. Y. Kim, S. J. Hwang, and C. H. Goo, "Shape design of the duct for tidal converters using both numerical and experimental approaches (pre-2015)," *Energies (Basel)*, vol. 9, no. 3, Mar. 2016, doi: 10.3390/en9030185.

[8] A. A. Rahman, K. Rajendran, A. Abdul-Rahman, G. E. Suhri, and L. Dass, "Analysis of Wake Turbulence for a Savonius Turbine for Malaysia's Slow-Moving Current Flow," *International Journal of Renewable Energy Development*, vol. 11, no. 4, pp. 1078–1088, Nov. 2022, doi: 10.14710/ijred.2022.45985.

[9] G. E. Suhri, A. Abdul Rahman, L. Dass, K. Rajendran, and A. Abdul Rahman, "INTERACTIONS BETWEEN TIDAL TURBINE WAKES: NUMERICAL STUDY FOR SHALLOW WATER APPLICATION," *J Teknol*, vol. 84, no. 4, pp. 91–101, May 2022, doi: 10.11113/jurnalteknologi. v84.17731.

[10] R. Hassanzadeh, O. bin Yaakob, M. M. Taheri, M. Hosseinzadeh, and Y. M. Ahmed, "An innovative configuration for new marine current turbine," *Renew Energy*, vol. 120, pp. 413–422, May 2018, doi: 10.1016/j.renene.2017.11.095.

[11] A. H. M. Din *et al.*, "Malaysian sea water level pattern derived from 19 years tidal data," *J Teknol*, vol. 79, no. 5, pp. 137–145, Jul. 2017, doi: 10.11113/jt.v79.9908.

[12] J. T. Park and A. Olivieri, "Recommended Procedures Fresh Water and Seawater Properties," in *International Towing Tank Conference*, 2011, p. 8.

[13] K. G. Nayar, M. H. Sharqawy, L. D. Banchik, and J. H. Lienhard, "Thermophysical properties of seawater: A review and new correlations that include pressure dependence," *Desalination*, vol. 390, pp. 1–24, Jul. 2016, doi: 10.1016/j.desal.2016.02.024.

[14] L. Dass, A. Abdul Rahman, K. Rajendran, and G. E. Suhri, "Numerical analysis of wake turbulence between hybrid tidal turbine and hypothetical actuator cylinder for shallow water with low velocity conditions," *Journal of Mechanical Engineering and Sciences*, vol. 16, no. 1, pp. 8673–8690, Mar. 2022, doi: 10.15282/jmes.16.1.2022.03.0686.

[15] D. Satrio and I. K. A. P. Utama, "Experimental investigation into the improvement of self-starting capability of vertical-axis tidal current turbine," *Energy Reports*, vol. 7, pp. 4587–4594, Nov. 2021, doi: 10.1016/j.egyr.2021.07.027.

[16] H. Faez Hassan, A. El-Shafie, and O. A. Karim, "Tidal current turbines glance at the past and look into future prospects in Malaysia," *Renewable and Sustainable Energy Reviews*, vol. 16, no. 8. pp. 5707–5717, Oct. 2012. doi: 10.1016/j.rser.2012.06.016.

[17] T. Stallard, R. Collings, T. Feng, and J. Whelan, "Interactions between tidal turbine wakes: Experimental study of a group of three-bladed rotors," *Philosophical Transactions of the Royal Society A: Mathematical, Physical and Engineering Sciences*, vol. 371, no. 1985, Feb. 2013, doi: 10.1098/rsta.2012.0159.

[18] V. Clary, T. Oudart, P. Larroudé, J. Sommeria, and T. Maître, "An optimally-controlled RANS Actuator force model for efficient computations of tidal turbine arrays," *Ocean Engineering*, vol. 212, Sep. 2020, doi: 10.1016/j.oceaneng.2020.107677.

[19] A. Olczak, T. Stallard, T. Feng, and P. K. Stansby, "Comparison of a RANS blade element model for tidal turbine arrays with laboratory scale measurements of wake velocity and rotor thrust," *J Fluids Struct*, vol. 64, pp. 87–106, Jul. 2016, doi: 10.1016/j.jfluidstructs.2016.04.001.

[20] K.-P. Kim, M. R. Ahmed, and Y.-H. Lee, "Efficiency improvement of a tidal current turbine utilizing a larger area of channel," *Renew Energy*, vol. 48, Dec. 2012, doi: 10.1016/j.renene.2012.06.018.